# An AlN/$Al_{0.85}Ga_{0.15}N$ high electron mobility transistor

Albert G. Baca, Andrew M. Armstrong, Andrew A. Allerman, Erica A. Douglas, Carlos A. Sanchez, Michael P. King, Michael E. Coltrin, Torben R. Fortune, and Robert J. Kaplar

Sandia National Laboratories

PO Box 5800, Albuquerque, NM 87185-1085 USA

Abstract: An AlN barrier high electron mobility transistor (HEMT) based on the AlN/$Al_{0.85}Ga_{0.15}N$ heterostructure was grown, fabricated, and electrically characterized, thereby extending the range of Al composition and bandgap for AlGaN channel HEMTs. An etch and regrowth procedure was implemented for source and drain contact formation. A breakdown voltage of 810 V was achieved without a gate insulator or field plate. Excellent gate leakage characteristics enabled a high $I_{on}/I_{off}$ current ratio greater than $10^7$ and an excellent subthreshold slope of 75 mV/decade. A large Schottky barrier height of 1.74 eV contributed to these results. The room temperature voltage-dependent 3-terminal off-state drain current was adequately modeled with Frenkel-Poole emission.

Material comparisons based on measures relating to conduction loss are widely used in comparing the attributes of radio frequency (rf) and power switching semiconductor devices. The lateral figure of merit [1], $LFOM = \frac{V_{br}^2}{R_{on,sp}} = q\mu n_s E_c^2$ , is appropriate for high electron mobility transistors (HEMTs), where $q$ is the electron charge, $\mu$ is the electron mobility, $n_s$ the sheet charge, $E_C$ the critical field for avalanche breakdown, $V_{br}$ is the off-state breakdown voltage, and $R_{on,\,sp}$ is the specific on-state resistance. It is the lateral device analog to a widely quoted unipolar *FOM* pertaining to conduction losses in one-sided abrupt junctions, $UFOM = \frac{V_{br}^2}{R_{on,sp}} = \frac{1}{4}\varepsilon\mu E_c^3$ [2],

where $\varepsilon$ is the dielectric constant. Although an imperfect *FOM* because performance metrics other than conduction loss also matter, comparisons to the *UFOM,* and by extension to the *LFOM* as well, are useful because it is widely used. Both the *UFOM* and the *LFOM* favor wide bandgap semiconductors such as GaN and SiC over Si and GaAs for rf and power electronics applications since the critical electric field is modeled to scale as $E_g^{2.5}$ (bandgap to the 2.5$^{th}$ power) [3]. Once envisioned as promising based on *UFOM* comparisons with GaAs and Si [4], HEMTs from AlGaN/GaN materials [5] are becoming the preferred technology for rf and power switching applications [6,7]. $Al_xGa_{1-x}N$ channel HEMTs with high x are relatively unexplored due to the technological difficulties associated with immature materials and fabrication in the high Al containing materials. $Al_xGa_{1-x}N$ channel HEMTs with x ranging from 0.15-0.60 have been reported [8-12] and breakdown voltage comparisons have been made against comparable GaN channel devices, but not yet at x-values expected to have a better *LFOM* than GaN-channel HEMTs. Simulations suggest that the *LFOM* for $Al_xGa_{1-x}N$ channels exceeds that for GaN channels for $x > 0.9$ at room temperature and at lower x for elevated temperatures [13], supporting the interest for investigating high x devices.

Although ref. [13] suggests that the *LFOM* for $Al_xGa_{1-x}N$ increases continually until x=1, the Al-composition of the AlGaN must be well matched to the AlN barrier layer of the HEMT, with a large enough conduction band offset to achieve a reasonable $n_s$. The assumption of constant $n_s$ ($=10^{13}$ cm$^{-2}$) breaks down for $x > 0.85$ because of insufficient conduction band offset to sustain that value of $n_s$. Therefore, the *LFOM* should reach its maximum value near x=0.85, the composition investigated in this study. In this letter, we report on the growth, fabrication, and dc characterization of a HEMT based on the $AlN/Al_{0.85}Ga_{0.15}N$ heterostructure, thereby extending the range of Al composition and bandgap for AlGaN channel HEMTs. A breakdown

voltage of 810 V was measured for this HEMT without the use of any sophisticated electric field management. These results illustrate the promise of ultra-wide bandgap devices for high-voltage power and rf electronics.

HEMT samples were grown by metal organic chemical vapor deposition (MOCVD) on sapphire substrates. The essential elements of the epitaxial structure consist of an AlN nucleation and buffer layer grown thick enough to planarize on a sapphire substrate, a 400 nm 85% Al containing AlGaN buffer and channel layer, and a 48 nm thick AlN barrier, all without intentional doping. The unintentionally doped AlN and $Al_{0.85}Ga_{0.15}N$ layers were confirmed to be electrically insulating from Hg-probe *CV* and contactless resistivity sheet resistance measurements of representative AlN and $Al_{0.85}Ga_{0.15}N$ thin films grown under nominally identical conditions and on nominally identical substrate and nucleation layers. This epitaxial structure anticipates the future need for a pseudomorphic structure with low dislocation density once AlN substrates are used. The charge transferred to the HEMT channel likely occurs by means of polarization doping, analogous to that in GaN channel and other piezoelectric heterostructures. Contactless resistivity measurements were carried out with a Lehighton instrument and resistivity of the conducting layer was as good as 4200 Ω per square. From *CV* measurements carried out with a mercury probe, a pinchoff voltage near -4 V and a sheet charge of $6x10^{12}$ $cm^{-2}$ were characterized. A mobility of 250 $cm^2V^{-1}s^{-1}$ was inferred from the sheet charge and resistivity according to the relation $\rho = (q\mu n_s)^{-1}$. Using the methods of ref. [13], we calculate a theoretical *LFOM* for the $Al_{0.85}Ga_{0.15}N$-channel HEMT that is 1.0x, 2.1x, and 3.1x that of a GaN-channel HEMT at 300K, 400K, and 500K, respectively. Since power and rf devices pushed to the limits of their performance undergo considerable self-heating, the greater than unity high temperature *LFOM* is noteworthy.

Circular HEMTs with gate length of 2.0 μm and circumference of 314 μm (defined at gate center) were fabricated using a process with six layers of photolithography. First, the source and drain contacts were prepared by dry etching the AlN barrier [14] and then re-growing $n^+$ GaN in place of the etched away AlN using an epitaxial lateral overgrowth (ELOG) style regrowth procedure by MOCVD with a SiN dielectric mask. High resolution scanning electron microscope images (not shown) provide evidence that the GaN:Si has grown conformally over the exposed AlGaN and AlN surfaces, reducing the likelihood that an exposed and depleted AlGaN surface may contribute substantially to parasitic resistance that we will attribute to the source and drain contacts. Second, source and drain contact metal deposition and alloy (850ºC) based on a commonly used Ti/Al/Ni/Au metal stack was carried out. Third, a Schottky gate metal with a Ni/Au metal stack was formed between the source and drain contact regions. Fourth, a SiN passivation and via etch was carried out. Fifth, a second Ni/Au metal stack was deposited for pad metal. Finally, a second SiN and via etch was deposited for further device passivation. A cross-section and top view of the device are illustrated in Figure 1.

Sample testing was carried out using a wafer prober, needle probes, and a semiconductor parameter analyzer. Breakdown measurements were carried out by immersing the sample and the needle probes in Fluorinert.

The electrical performance of the HEMT is illustrated in Figures 2 and 3. In Figure 2, the drain current is plotted against the drain voltage for gate voltages ranging from $V_{GS}$ = -6 V to $V_{GS}$ = 3V using +1V gate voltage steps. A gate voltage above 3V was not used because the source-to-gate diode turns on at approximately 2.2 V and can begin to negatively affect the test results. An offset voltage is apparent because the source and drain contacts are not strictly linear at low voltages, but instead shows some evidence of rectifying behavior. Nevertheless, the shape of the

$I_{DS}$-$V_{DS}$ characteristic is otherwise similar to that expected for HEMTs, such as those using AlGaN/GaN materials. The maximum current attained in these devices is almost three orders of magnitude lower than the norm for GaN/AlGaN HEMTs, an observation that is analyzed further below. Trapping effects, expected in wide bandgap semiconductors, are evidenced by both an observed light sensitivity and hysteresis in the $I_{DS}$-$V_{DS}$ curves, whereby $I_{DS}$-$V_{DS}$ curves scanned from high $V_{GS}$ to low $V_{GS}$ (not shown) result in higher $I_{max}$ than those scanned from low $V_{GS}$ to high $V_{GS}$.

In Figure 3, the drain current is plotted against the gate voltage for a drain voltage of 10 V. The drain current decreases exponentially in the subthreshold region, with an exceptionally good subthreshold slope of 75 mV per decade. On a linear scale (not shown), the $I_{DS}$-$V_{GS}$ plot is quadratic in the on-state and the threshold voltage was measured to be -4.9 V using the intercept of the $\sqrt{I_{DS}}$ vs. $V_{GS}$ plot. The minimum off-state leakage current is very low and near the noise level of the electrical test equipment. The on-off current ratio, $I_{on}/I_{off}$, of greater than $10^7$ is evident from Figure 3 and is indicative of a high quality device.

The gate current corresponding to the plots of Figure 2 (not shown) and Figure 3 is extremely low, often near 10 pA, and nearly invariant with bias conditions associated with on-state operation. These excellent results for 3-terminal drain and gate leakage currents even extend to scans to much higher drain voltage, discussed further below and indicates the quality of the AlN barrier, the Schottky contact, and the AlGaN buffer. The temperature dependent forward biased gate-drain $I$-$V$ curves are shown in Figure 4. The Ni/Au Schottky barrier height of 1.74 eV, extracted by the methods of reference [15], is higher than that for n-GaN (0.99 eV) and $Al_{0.25}Ga_{0.75}N$/GaN (1.27 eV) [16], as expected, and contributes to the excellent gate leakage

properties in AlN/AlGaN HEMTs, while gate leakage remains problematic for Schottky gates on AlGaN/GaN HEMTs[17-21].

Dielectric barriers including $SiO_2$ [22], SiN [23], and $Al_2O_3$ [24] have been shown to reduce gate and 3-terminal drain leakage currents in the AlGaN/GaN HEMTs, while no similar reports achieve similarly low gate leakage using Schottky barrier contacts. Chung et al. have reported that gate current in GaN/AlGaN HEMTs with Ni/Au/Ni Schottky gates can be reduced more than 4 orders of magnitude by means of an oxide plasma treatment that leads to a self-limiting thickness of $Ga_2O_3$ acting as a gate dielectric between the Schottky gate and the AlGaN [25]. Such a reduction in gate leakage leads to a correspondingly low 3-terminal drain current in the off-state as well as a reduction in the subthreshold slope from 176 mV/decade to 64 mV/decade [25]. The AlN/AlGaN HEMT from this work achieves similarly impressive leakage metrics while using a Schottky contact.

The three-terminal breakdown characteristics are illustrated in Figure 5, where a logarithmic plot of drain and gate currents versus drain voltage is shown for a 10 μm gate-drain separation. A few observations are in order. The drain current is measured using a high voltage SMU with a noise floor of 1 nA, while the gate current is measured using a sensitive low current SMU capable of measuring pA current levels. Below 200 V, the drain current is below the noise limit of the measurement system. The gate current is at or close to the noise limit until the drain voltage approaches 200 V and then increases with a higher slope than the drain current, while remaining lower than the drain current until breakdown at 810 V. Between $V_{DS}$ of 205-715 V, the drain current fits the bias dependence for Frenkel-Poole emission current as seen in Figure 5, and the gate current does not. At constant temperature, Frenkel-Poole emission is modeled simply as $I = AVe^{\sqrt{BV}}$ where V is the drain voltage and A and B are temperature dependent constants,

with the best fit for $A=1.1x10^{-12}$ $V^{-1}$ and $B=5.0x10^{-4}$ $V^{-1}$. Normally, Frenkel-Poole emission is an important element of the gate current dependence with gate bias in AlGaN/GaN HEMTs with Schottky gates [26]. The results of Figure 5 suggest that a current path other than gate electrode electrons populating AlN barrier traps for Frenkel-Poole emission is operative in the AlN/AlGaN HEMTs. This alternative current path is possibly related to the abrupt conduction band offset associated with the regrown source and drain contacts, whereby an AlGaN trap's electron emission near the regrown contact region is the source of the Frenkel-Poole emission and the Fermi level of the GaN:Si region is the source of electrons. A detailed investigation of the conducting mechanisms for both gate and drain currents requires considerably more temperature dependent measurements, analysis, and modeling, and will be the subject of a follow-up publication.

These breakdown results pertain to a device with a standard gate geometry and no sophisticated electric field management (e.g. no field plate in the gate-drain access region). They compare against a recently reported value of 755 V for another ultra-wide bandgap semiconductor based on a $\beta$-$Ga_2O_3$ FET of comparable maturity [27], though still not reaching the 1.65-1.7 kV reported for previous AlGaN channel HEMTs with lower Al composition using a field plate [8,11]. The $Al_{0.85}Ga_{0.15}N$ channel HEMT of this work without a fieldplate has a larger breakdown voltage compared to AlGaN/GaN HEMTs with a fieldplate of reference [11], but comparable to other published results with a 10 μm gate-drain separation [28].

Next we present evidence that the limited current density achieved in the HEMTs of this work arises from high source and drain contact resistance that otherwise belies the promise of such HEMTs. First, the $I_{DS}$-$V_{DS}$ plot below the knee is supposed to be linear if dominated by channel mobility but is instead quadratic in shape. Second, all $I_{DS}$-$V_{DS}$ curves below the knee

voltage overlay nearly perfectly, but a textbook HEMT with a low voltage $I_{DS}$-$V_{DS}$ slope that is determined by channel mobility inferred from the relation $I_{DS} = q\mu n_s E$ should show that gate voltage modulates the channel conductivity through $n_s$. In fact, using the electron mobility of 250 $cm^2$/V-s and maximum sheet charge of $6x10^{12}$ $cm^{-2}$ inferred from *C-V* and sheet resistance measurements, a saturation current > 100 mA/mm should be possible for the geometry of Figure 1. Third, neither gateless HEMTs nor TLMs showed a current dependence on contact separation. Rather, a gateless HEMT only reaches 10 mA/mm at 40 V. A contact resistivity of approximately 1900 Ω–mm was estimated from the gateless HEMT results. Although high in resistance, source and drain contacts with GaN:Si regrowth are more than $10^3$ times better than planar contacts from our laboratory [14].

Prior work on high Al-containing AlGaN channel HEMTs have shown contact-limited current or extraordinary measures to address Ohmic contact limitations [8-12], not inconsistent with the need for a special contact regrowth in the present work. For example, Tokuda *et al.* developed Zr-based Ohmic contacts [9] for HEMT barrier layers containing 86% Al with a channel containing 51% Al and Nanjo *et al.* realized good contacts by means Si ion implantation with a 1150C anneal for HEMT barrier layers containing 40% Al with a channel containing 20% Al [11]. Even so, these prior HEMT publications, which represent state-of-the-art work, show a hint of an offset voltage in the HEMT $I_{DS}$-$V_{DS}$ characteristics and contact resistivity demonstrably worse than typical for AlGaN/GaN.

The high contact resistance mainly affects the on-state HEMT properties and does not artificially raise the breakdown voltage. The 810 V breakdown voltage demonstrated is high by absolute standards, but corresponds to an average of 0.81 MV/cm, which is only a fraction of the predicted $E_C$ in $Al_{0.85}Ga_{0.15}N$ (estimated at 11 MV/cm). The theoretical $E_C$ nevertheless offers

considerable promise for the ultimate performance of $Al_{0.85}Ga_{0.15}N$ channels in light of its weighting in the lateral figure of merit.

In summary, we have demonstrated the growth, fabrication, and electrical properties of an $AlN/Al_{0.85}Ga_{0.15}N$ HEMT. The breakdown voltage of 810 V, excellent gate leakage, the high $I_{on}/I_{off}$ current ratio greater than $10^7$, and excellent subthreshold slope of 75 mV/decade illustrate the promise of these ultra-wide bandgap devices. The source and drain contact difficulty remains a challenge for these types of devices.

Acknowledgements: The authors thank Jennifer Barrios, Karen Cross, and Vincent Abate for fabrication and materials support and Christopher Nordquist for fruitful discussions and for reviewing the manuscript. This work was supported by the Laboratory Directed Research and Development (LDRD) program at Sandia. Sandia National Laboratories is a multi-program laboratory managed and operated by Sandia Corporation, a wholly owned subsidiary of Lockheed Martin Corporation, for the U.S. Department of Energy's National Nuclear Security Administration under contract DE-AC04-94AL85000.

References:


1. N. Zhang, Ph.D. thesis, University of California, Santa Barbara, 2002.
2. K. Shenai, R. S. Scott and B. J. Baliga, IEEE T. Electron. Dev. **36**, 1811 (1989).
3. J. L. Hudgins, G. S. Simin, E. Santi and M. A. Khan, IEEE T. Power Electr. **18**, 907 (2003).
4. U. K. Mishra, P. Parikh and W. Yi-Feng, Proc. IEEE **90,** 1022 (2002).
5. M. Asif Khan, A. Bhattarai, J. N. Kuznia and D. T. Olson, Appl. Phys. Lett. **63**, 1214 (1993).
6. U. K. Mishra, L. Shen, T.E. Kazior, and Y.-F. Wu, Proc. IEEE 96, 2 (2008).
7. S. Chowdhury, B. L. Swenson, M.H. Wong, U.K. Mishra, Semicond. Sci. Technol. 28, 074014 (2013).
8. T. Nanjo, M. Takeuchi, M. Suita, T. Oishi, Y. Abe, Y. Tokuda and Y. Aoyagi, Appl. Phys. Lett. **92**, 263502 (2008).
9. H. Tokuda, M. Hatano, N. Yafune, S. Hashimoto, K. Akita, Y. Yamamoto and M. Kuzuhara, Appl. Phys. Exp. **3**, 121003 (2010).
10. N. Yafune, S. Hashimoto, K. Akita, Y. Yamamoto and Kuzuhara, Jpn. J. Appl. Phys. **50**, 100202 (2011).
11. T. Nanjo, A. Imai, Y. Suzuki, Y. Abe, T. Oishi, M. Suita, E. Yagyu and Y. Tokuda, IEEE T. Electron. Dev. **60**, 1046 (2013).
12. N. Yafune, S. Hashimoto, K. Akita, Y. Yamamoto, H. Tokuda and M. Kuzuhara, Electron. Lett. **50**, 211 (2014).
13. S. Bajaj, T.-H. Hung, F. Akyol, D. Nath and S. Rajan, Appl. Phys. Lett. **105**, 263503 (2014).
14. E. A. Douglas, A.A. Allerman, C.A. Sanchez, A.G. Baca, "Inductively Coupled $BCl_3/Cl_2$/Ar Plasma Etching of High Al Content AlGaN," *To Be Published* (2016).
15. A. C. Schmitz, A. T. Ping, M. A. Khan, Q. Chen, J. W. Yang and I. Adesida, Semicond. Sci. Technol. **11**, 1464 (1996).
16. Z. Lin, W. Lu, J. Lee, D. Liu, J. S. Flynn and G. R. Brandes, Appl. Phys. Lett. **82**, 4364 (2003).
17. E. J. Miller, X. Z. Dang and E. T. Yu, J. Appl. Phys. **88**, 5951 (2000).
18. H. Zhang, E. J. Miller and E. T. Yu, J. Appl. Phys. **99**, 023703 (2006).
19. E. J. Miller, E. T. Yu, P. Waltereit and J. S. Speck, Appl. Phys. Lett. **84**, 535 (2004).
20. M. Shinya, O. Yutaka, K. Shigeru, M. Koichi and M. Takashi, Jpn. J. Appl. Phys. **41**, 5125 (2002).
21. S. Arulkumaran, T. Egawa, H. Ishikawa and T. Jimbo, Appl. Phys. Lett. **82**, 3110 (2003).
22. M. A. Khan, X. Hu, G. Sumin, A. Lunev, J. Yang, R. Gaska and M. S. Shur, IEEE Electr. Device L. **21**, 63 (2000).
23. X. Hu, A. Koudymov, G. Simin, J. Yang, M. A. Khan, A. Tarakji, M. S. Shur and R. Gaska, Appl. Phys. Lett. **79**, 2832 (2001).
24. S. Ootomo, T. Hashizume and H. Hasegawa, Phys. Status Solidi C **0**, 90 (2003).
25. J. W. Chung, J. C. Roberts, E. L. Piner and T. Palacios, IEEE Electr. Dev. L. **29**, 1196 (2008).
26. S. Turuvekere, N. Karumuri, A. A. Rahman, A. Bhattacharya, A. DasGupta and N. DasGupta, IEEE T. Electron Dev. **60**, 3157 (2013).
27. M. H. Wong, K. Sasaki, A. Kuramata, S. Yamakoshi, and M. Higashiwaki, IEEE Electr. Device L. **37**, 212 (2016).
28. Y. Dora, A. Chakraborty, L. McCarthy, S. Keller, S. P. DenBaars, and U. K. Mishra, IEEE Electr. Device L. **27**, 713 (2007).

Figure captions:

Figure 1. A cross sectional diagram (a) and top view (b) illustrating the HEMT structure and geometry (not to scale). The horizontal dashed line of (b) shows the cut line for the cross section in (a).

Figure 2. Drain current vs. drain voltage for an AlN/$Al_{0.85}Ga_{0.15}N$ HEMT.

Figure 3. Drain and gate current vs. gate voltage for an AlN/$Al_{0.85}Ga_{0.15}N$ HEMT for $V_{DS}$ = 10V.

Figure 4. Gate diode current vs. gate voltage at various temperatures for Schottky barrier determination for an AlN/$Al_{0.85}Ga_{0.15}N$ HEMT.

Figure 5. Drain and gate current vs. drain voltage for an AlN/$Al_{0.85}Ga_{0.15}N$ HEMT for $V_G$ = -6 V showing a breakdown voltage of 810 V and a good fit of drain current to Frenkel-Poole emission from 205-715 V.

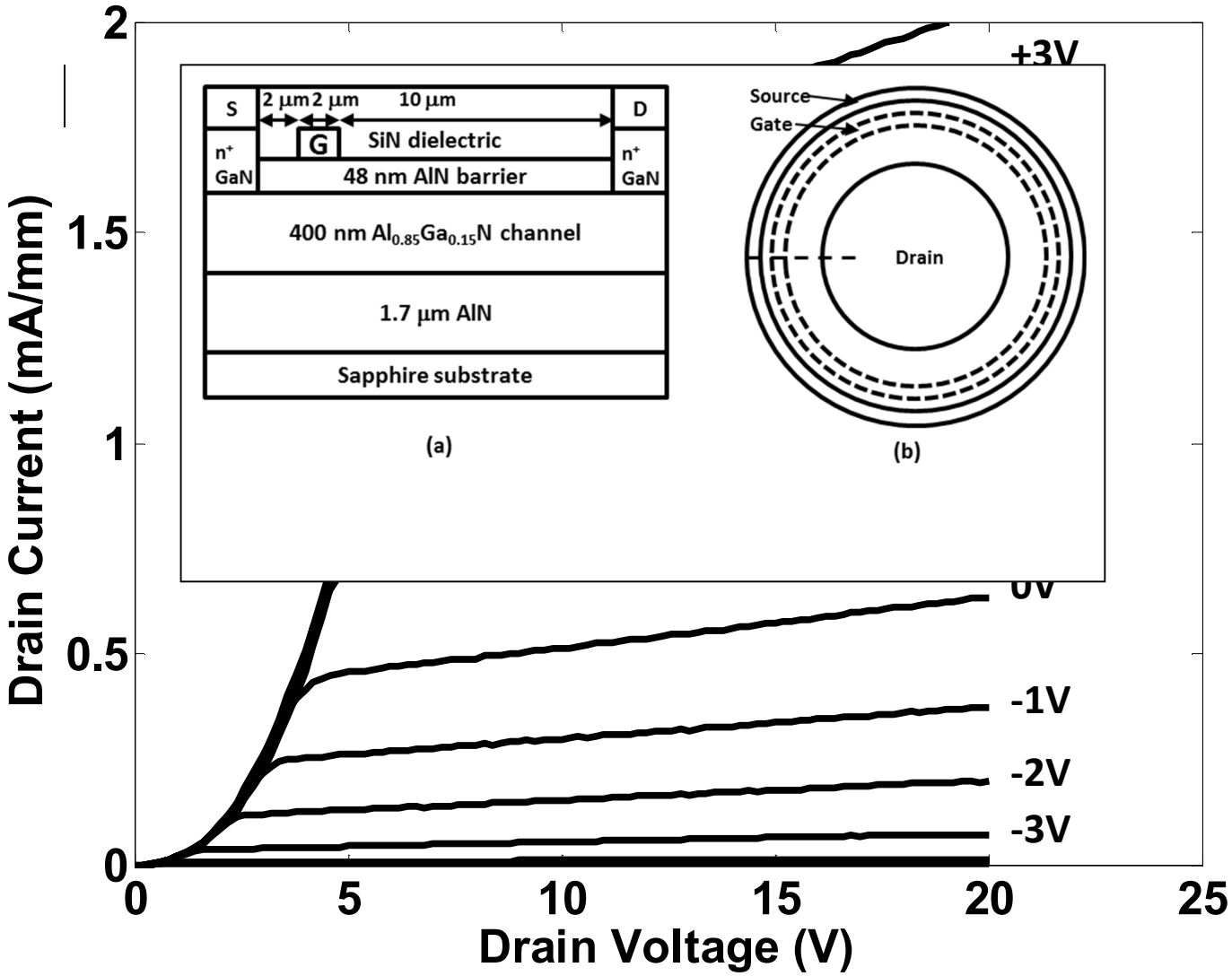
Drain Current (mA/mm)
Drain Voltage (V)
+3V
0V
-1V
-2V
-3V
S
D
2 μm
2 μm
10 μm
G
SiN dielectric
n+ GaN
48 nm AlN barrier
n+ GaN
400 nm Al0.85Ga0.15N channel
1.7 μm AlN
Sapphire substrate
(a)
Source
Gate
Drain
(b)

**Figure 2**

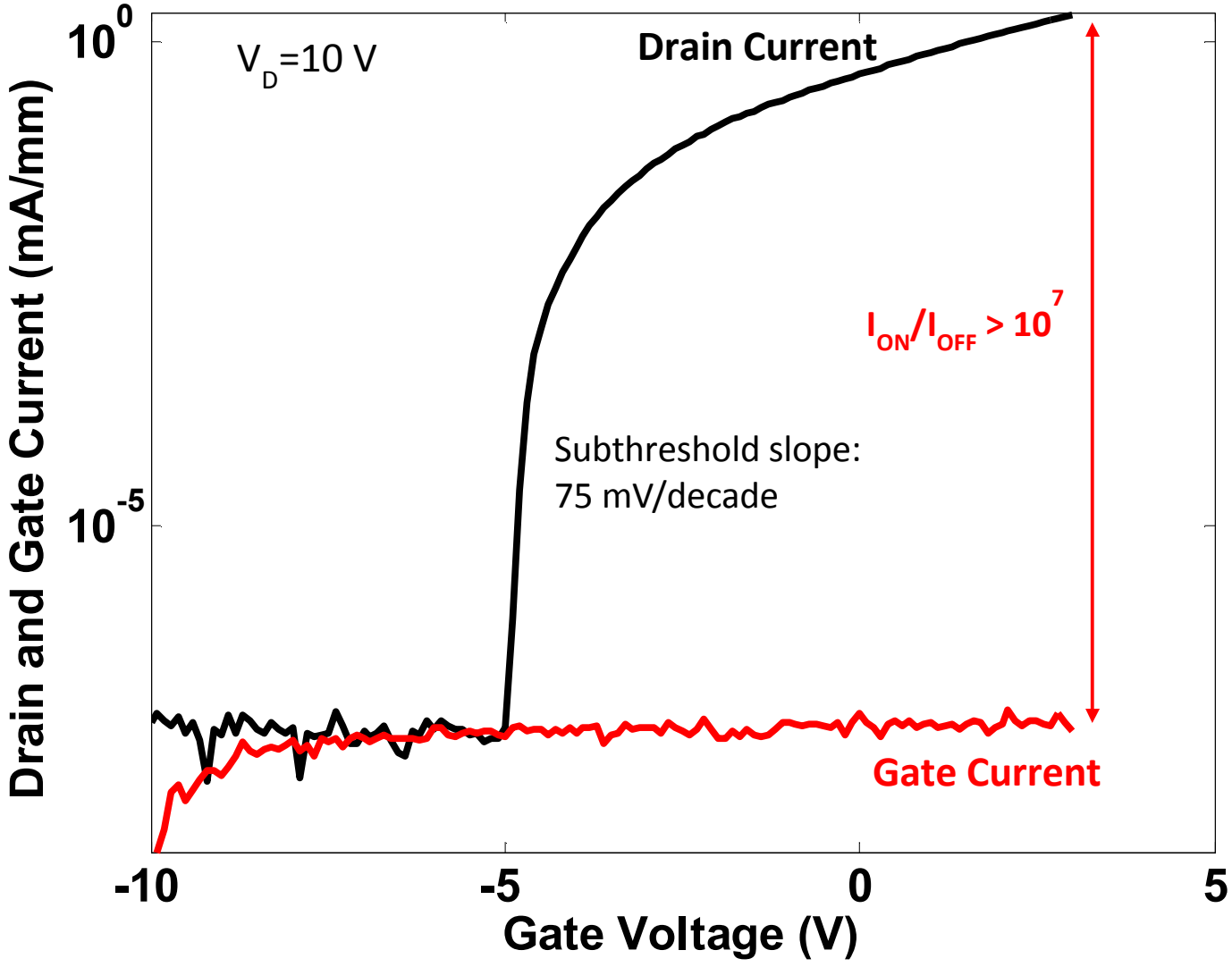
$10^0$
$10^{-5}$
$V_D$=10 V
Drain Current
$I_{ON}/I_{OFF} > 10^7$
Subthreshold slope:
75 mV/decade
Gate Current
Drain and Gate Current (mA/mm)
-10
-5
0
5
Gate Voltage (V)

**Figure 3**

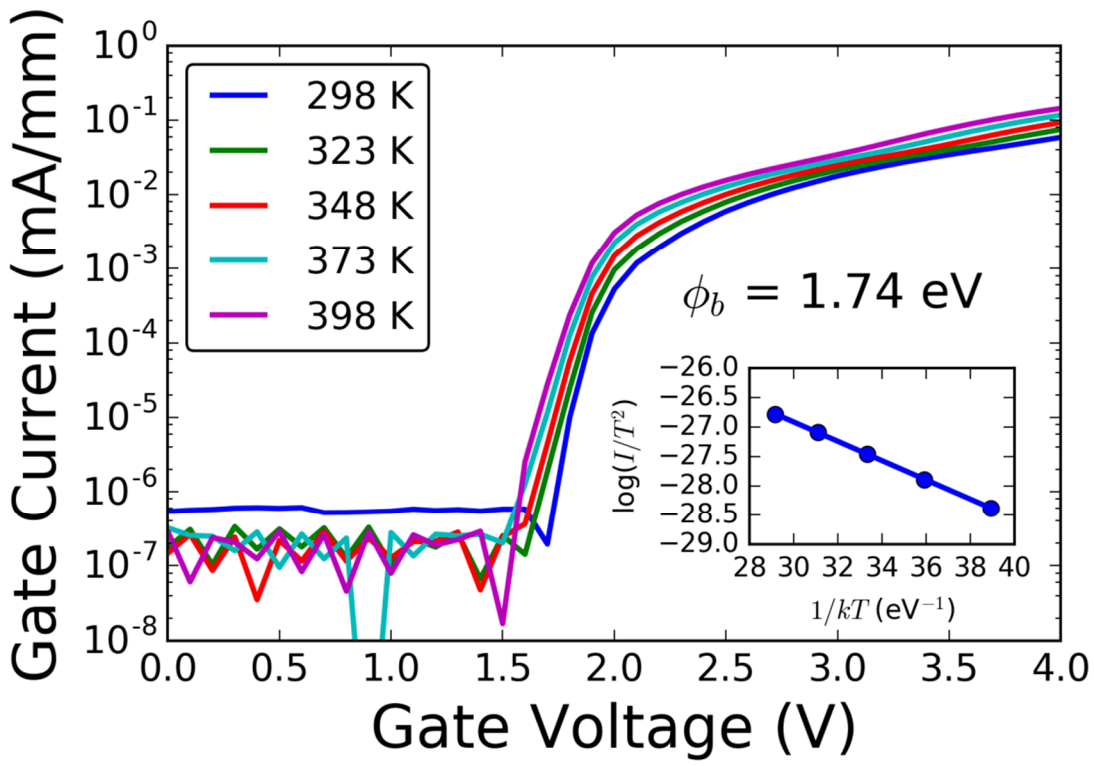
Gate Current (mA/mm)
Gate Voltage (V)
298 K
323 K
348 K
373 K
398 K
$\phi_b$ = 1.74 eV
$\log(I/T^2)$
$1/kT$ (eV$^{-1}$)

Figure 4.

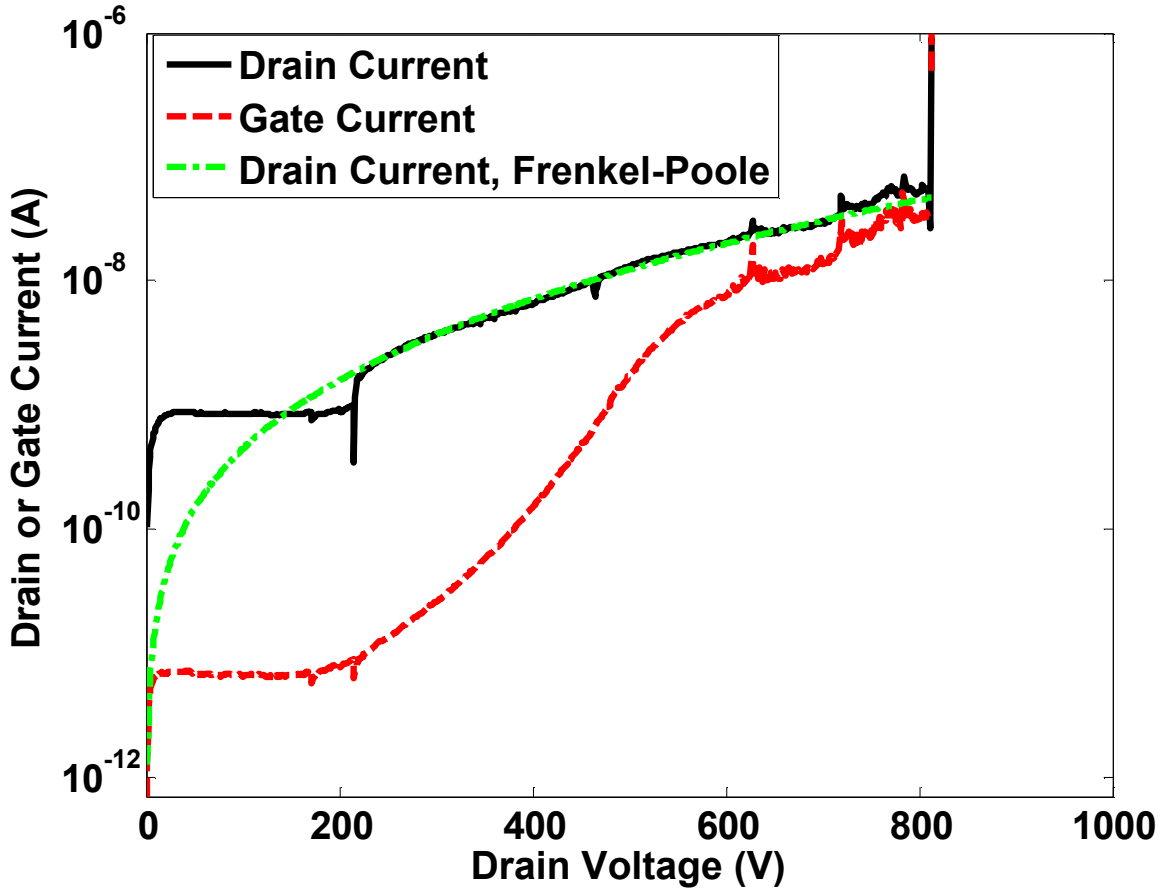
Drain Current
Gate Current
Drain Current, Frenkel-Poole
Drain or Gate Current (A)
10^-6
10^-8
10^-10
10^-12
0
200
400
600
800
1000
Drain Voltage (V)

Figure 5.